G Model
NSM-6119; No. of Pages 10
ARTICLE IN PRESS
Journal of Neuroscience Methods xxx (2011) xxx–xxx
Contents lists available at SciVerse ScienceDirect
Journal of Neuroscience Methods
journal homepage: www.elsevier.com/locate/jneumeth

Adaptive estimation of EEG-rhythms for optimal band identification in BCI

Kalyana C. Veluvolu*, Yubo Wang, Swathi S. Kavuri

School of Electronics Engineering, College of IT Engineering, Kyungpook National University, Daegu 702-701, Republic of Korea

ARTICLE INFO

Article history:
Received 4 February 2011
Received in revised form 23 August 2011
Accepted 23 August 2011

Keywords:
EEG classification
Time-frequency analysis
Adaptive estimation
BCI

ABSTRACT

The amplitude of EEG μ-rhythm is large when the subject does not perform or imagine movement and attenuates when the subject either performs or imagines movement. The knowledge of EEG individual frequency components in the time-domain provides useful insight into the classification process. Identification of subject-specific reactive band is crucial for accurate event classification in brain–computer interfaces (BCI). This work develops a simple time-frequency decomposition method for EEG μ rhythm by adaptive modeling. With the time-domain decomposition of the signal, subject-specific reactive band identification method is proposed. Study is conducted on 30 subjects for optimal band selection for four movement classes. Our results show that over 93% the subjects have an optimal band and selection of this band improves the relative power spectral density by 200% with respect to normalized power.

1. Introduction

The brain–computer interface (BCI) is an emergent technology that provides a new pathway for communication by allowing the brain to control a computer directly, without any physical movement achieved through normal neuromuscular pathways (Wolpaw et al., 2000; Comment, 2006). Non-invasive EEG-based BCIs for neuroprosthesis control has been an attractive control method for various applications ranging from cursor control to robotic neuroprosthesis (Wolpaw et al., 2000; Graimann et al., 2010; Schalk and Mellinger, 2010; Mueller-Putz et al., 2006, 2000; Sun et al., 2000). Among the various ways to acquire brain signals, EEG still remains as the most viable option (Wolpaw et al., 2000; Curran and Strokes, 2003; Vaughan, 2000). The analysis for EEG signal can be performed in both time and frequency domains. Both forms of analysis can be used for EEG-based communication (Wolpaw et al., 2000).

Spatial filters (Blankertz et al., 2008) that match the spatial frequencies of the users μ or β rhythms, autoregressive frequency analysis (McFarland et al., 2008; McFarland and Wolpaw, 2008) that gives higher resolution than fast Fourier transform (FFT) analysis for short time segments to permit rapid device control are popular for BCI applications. Frequency-domain control based on μ and β rhythms can be combined with time-domain control based on slow potentials to yield better EEG-based communication (McFarland et al., 1997; Krusienski et al., 2007; Brunner et al., 2010; Guger et al., 2003). If the data is available for short time segments, the frequency domain classification via band-power may not accurate.

In Neuper et al. (2000), it was shown that by estimating the band power in the frequency band (15–19 Hz) and by applying simple threshold classification, the foot motor imagery related brain pattern could be detected with 100% accuracy. The amplitude of the μ rhythm is largest when the subject is not moving or not imagining any movement, and attenuates when the subject is moving or imagines movement (Wolpaw et al., 2000; Birbaumer et al., 1999; Pfurtscheller et al., 2000; Pineda et al., 2000; Lotte et al., 2007). Movement-based BCI's recognize changes in the human μ rhythm from the central region of the scalp overlying the sensorimotor cortices (Comment, 2006; Mueller-Putz et al., 2006; Pineda et al., 2000). The free-running EEG shows characteristic changes in μ-activity, which are unique for the movement of different limbs (Pfurtscheller and Neuper, 2000). Studies that show that people can learn to regulate EEG μ-rhythm (Mueller-Putz et al., 2000; Pfurtscheller and Neuper, 2000; McFarland et al., 1997).

In general, the collected EEG signal is then divided into small segments, and the μ (8–13 Hz) and β (18–27 Hz) powers in each segment are calculated using frequency domain methods such as fast-Fourier-transform (FFT), autoregressive spectral analysis to calculate band-power for event classification. These methods rely on band power to classify the μ rhythm in the range of 8–13 Hz. A threshold is set for classifying the type of activity based on the rhythm (Guger et al., 2003; Neuper et al., 2000). As the band remains fixed for all subjects, large data sets are required for setting the threshold for classification.

Instead of using the complete μ or β spectral bands, narrowed subject-specific frequency bands are selected to achieve higher accuracy in classification (McFarland and Wolpaw, 2008; McFarland et al., 2010; Royer et al., 2000; Schalk and Mellinger, 2010). In McFarland and Wolpaw (2008), spectral bands with multiple 3 Hz-bins are selected for feature extraction to control cursor

* Corresponding author. Tel.: +82 539507232.
E-mail address: veluvolu@ee.knu.ac.kr (K.C. Veluvolu).

0165-0270/$ – see front matter © 2011 Elsevier B.V. All rights reserved.
doi:10.1016/j.jneumeth.2011.08.035

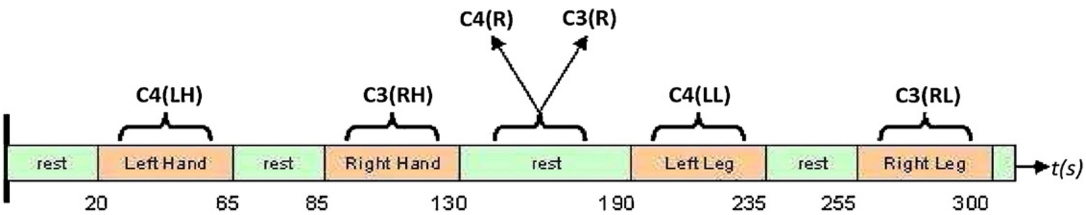

Fig. 1. EEG recording sequence and timings of the 5 classes in each trial.

movements. Recently, similar approach was adopted for three-dimensional movement in virtual space (McFarland et al., 2010; Royer et al., 2000). Tools to customize frequency band for subjects are readily available with BCI2000 (Schalk and Mellinger, 2010). However, in order to identify the subject specific reactive bands, large number of trials/training sessions are needed to identify the bands for electrode locations. These methods rely on higher-order (e.g. 16-order McFarland et al., 2010; Royer et al., 2000) autoregressive algorithm to model the EEG data. The data in short-time segments is processed and logarithmic amplitudes are employed as commands for control. In Blankertz et al. (2008), a heuristic approach was adopted for selection of discriminative spectral band. Methods that on auto-regressive spectral analysis or FFT based spectral estimation methods that does not provide temporal information. Time-domain (temporal) information of the dominant spectral bands is necessary for customizing subject-specific reactive band for a given electrode location.

Several time-frequency decomposition methods, such as band-pass filtering, short time Fourier transform and continuous wavelet transform, are analyzed for EEG analysis (Allen and MacKinnon, 2010; McFarland et al., 2008). In the band-pass filtering approach, the temporal resolution mainly depends on the filter type and the filter complexity increases with the spectral resolution. In the short time Fourier transform, the spectral and temporal resolution is pair of contradictory which depends on the time window selection. Recently, it was demonstrated in Allen and MacKinnon (2010) that continuous wavelet transform (CWT) is not superior to the STFT in terms of spectral and temporal resolution. Also its high-computation requirement remains as a barrier for real-time BCI applications. Auto-regressive methods (McFarland and Wolpaw, 2008; Bashashati et al., 2007) and Fourier transform (FFT) are popular for EEG spectral analysis that only provides spectral information but lack temporal resolution.

A simple and efficient method that provides optimal temporal and spectral resolution is required for real-time feature extraction in BCI. This paper develops a time-domain analysis method by estimation of bandlimited EEG μ-rhythm through adaptive filtering (Veluvolu and Ang, 2000). The method developed in (Veluvolu and Ang, 2000) is adopted to model the EEG signal through multiple Fourier series as individual frequency components with LMS algorithm. Compared to FFT, the proposed method does not rely on transformation and provides the individual frequency components in time-domain with optimal temporal resolution and user-defined frequency resolution.

With time-frequency decomposition obtained, a study is conducted on 30 subjects for optimal band identification that demonstrates the significant change in amplitude for accurate event classification. The study also aims to identify the characteristics of reactive band for different electrode locations for various movement classes. The time-domain characteristics of subjects reactive band for different movement classes will be crucial to identify an optimal band (common reactive band) for the subject. A measure is formulated based on the average energy distribution in the reactive band for 30 subjects with different movement classes. With this measure, a procedure to automatically identify the optimal band is presented. The study shows that selecting the optimal band for the subject increased the relative power spectral density by 200%.

2. Methods

Three channels EEG data were recorded monopolarly from C3, C4 and Cz corresponding to the international 10/20 system (Jasper, 1958), with the right mastoid as ground and left mastoid as reference. Analog-to-digital conversion and amplification of the EEG data was done by LXE3204 of LAXTHA (www.laxtha.com) which can provide 4 channels EEG data recording with one reference and one ground additionally. The data was sampled at 512 Hz.

34 subjects (12 female, 22 male) aged between 22 and 27 participated in the research study. All of the subjects are healthy and none of them has prior knowledge about EEG data collection. The subjects sat on a comfortable chair to make sure their limbs were in rest position. All participants gave written informed consent prior to study procedures. The study was approved by the Kyungpook National University Ethical Committee.

Four trials were recorded for each subject in one session. During the trial, 5 classes of movement were carried out: resting, left hand movement, right hand movement, left leg movement, and right leg movement. The sequence of each trial is shown in Fig. 1. Subjects were not informed of the sequence and the interval of each activity in order to minimize anticipatory actions. Each action began with an acoustic stimulus lasted 0.5 s followed by a picture and textual description shown on 26′′ computer screen to indicate the appropriate limb movement. The experiment setup is shown in Fig. 2. The data used for the comparison between various classes lasted 25 s, starting 10 s after the start of each class. For e.g. data in the segment C4(LH) (shown in Fig. 1) from 30 s to 55 s is considered for analysis. For rest, C4(R) or C3(R) segment data from time 140 s to 165 s is considered. Among 34 subjects, only 30 subjects (10 female, 20 male) data was used in the study. An observer stationed behind the

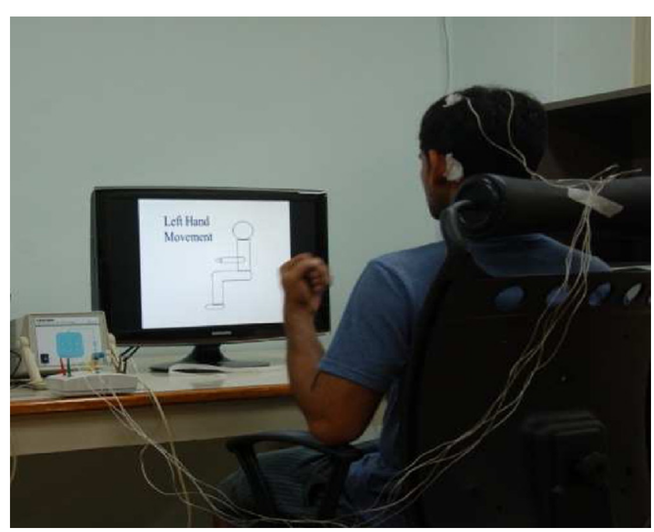

Fig. 2. Recording of EEG from a subject.

subject verified whether the desired movement instructed on the screen was performed by the subject. No feedback was provided to the subject about the movement performed. Four subjects failed to perform the required movement or performed no movement in at least two trials. When a subject fails to perform a minimum of 2 trials correctly, the subject data was excluded from the study. However, in the 30 subjects data chosen for analysis, 5 subjects in one or two trials failed to follow the instruction and performed a wrong movement or no movement. These trials were identified and the improper segments were removed from the data for analysis.

Subjects participated in two conditions:

(1) *Rest:* in which subjects sat in a chair comfortably and placed their hands on the table; a blank screen was shown, and they were instructed not to think of anything.
(2) *Self-generated movement:* subjects were cued to move his left/right hand or left/right leg at their own pace with a beep and on screen instructions.

2.1. Bandlimited multiple Fourier linear combiner (BMFLC)

Since EEG is comprised of quasi-periodic or quasi-sinusoidal signals characterized by coupled, harmonically related frequencies, there have been several Fourier based works (Akim and Kiymik, 2000; Krusienski et al., 2007; Brunner et al., 2010). A parameterized μ-rhythm model has been formulated with a matched filter for accurate tracking with harmonically related phase-coupled sinusoidal components (Krusienski et al., 2007; Brunner et al., 2010).

In this paper, we focus on bandlimited Fourier linear combiner based on LMS algorithm to estimate/track the μ-rhythm. Fourier linear combiner (FLC) (Vaz and Thakor, 2000; Vaz et al., 2000) is an adaptive filter that forms a dynamic truncated Fourier series model of an input signal. The FLC operates by adaptively estimating the Fourier coefficients of the known frequency model according to the LMS algorithm. To overcome the drawbacks in tracking bandlimited signals, the band limited multiple Fourier combiner is developed to track modulated signals (Veluvolu and Ang, 2000).

In order to estimate the unknown μ-rhythm, we consider the signal to be distributed in the band of $[\omega_1 - \omega_n]$ and then divide the frequency band of interest into 'n' finite number of divisions as shown in Fig. 3(b). For the estimation of the unknown signal, we then choose a series comprising of sine and cosine components to form band-limited multiple-Fourier linear combiner (BMFLC):

$$y_k = \sum_{r=1}^{n} a_{rk} \sin(\omega_r k) + b_{rk} \cos(\omega_r k) \tag{1}$$

where y_k denotes the estimated signal at sampling instant k. a_{rk}, b_{rk} represents the adaptive weights corresponding to the frequency ω_r at instant k. The following series only considers 'n' fundamental frequencies in the band. The division of the band, step size $\Delta\omega$ (in Fig. 3(b)) and selection of the fundamental frequencies will be presented in the later part of the section. We then adopt the LMS algorithm (Widrow and Stearns, 1985) to adapt the weights a_{rk}, b_{rk} in (1) to the incoming unknown signal. The architecture of the proposed algorithm is shown in Fig. 3(a). The algorithm can be stated as follows:

$$\mathbf{x}_k = \left\{ \begin{array}{l} [\,\sin(\omega_1 k) \quad \sin(\omega_2 k) \quad \ldots \quad \sin(\omega_n k)\,]^T \\ [\,\cos(\omega_1 k) \quad \cos(\omega_2 k) \quad \ldots \quad \cos(\omega_n k)\,]^T \end{array} \right\} \tag{2}$$

$$y_k = \mathbf{w}_k^T \mathbf{x}_k \tag{3}$$

$$\epsilon_k = s_k - y_k \tag{4}$$

$$\mathbf{w}_{k+1} = \mathbf{w}_k + 2\eta \mathbf{x}_k \epsilon_k \tag{5}$$

where

$$\mathbf{w}_k = [\, a_{1k} \quad \ldots \quad a_{nk} \quad b_{1k} \quad \ldots \quad b_{nk}\,]^T \tag{6}$$

and $\mathbf{x}_k$ are the adaptive weight vector and reference input vector respectively. s_k is the reference signal, ϵ_k represents the error term and η is an adaptive gain parameter. Input signal amplitude and phase are estimated by the adaptive vector $\mathbf{w}_k$.

From the architecture, it is clear that n-FLC's are combined to form BMFLC to estimate bandlimited signal. Since we select a band of frequencies, the corresponding weights adapt to the frequencies present in the input signal. Due to the LMS algorithm, the corresponding weights adapt to the change in frequency of the incoming signal. The adaptive gain parameter η can be chosen to have fast convergence without loosing stability. The stability of the algorithm can be established similar to (Vaz and Thakor, 2000). As the functions in $\mathbf{x}_k$ (2) are orthogonal with a mean power of 1/2 for each function, the autocorrelation matrix of $\mathbf{x}_k$ becomes diagonal and can be obtained as

$$\mathbf{R} = E[\, \mathbf{x}_k \quad \mathbf{x}_k^T\,] = \frac{1}{2}\mathbf{I} \tag{7}$$

According to Widrow and Stearns (1985), the practical bound for convergence is given by

$$0 < \eta < \frac{1}{tr[\mathbf{R}]} = 1/n \tag{8}$$

where $tr[\cdot]$ represents the trace of the matrix. Hence, for the BMFLC algorithm the adaptive gain parameter η should be less than $1/n$ to achieve convergence.

Since the objective is to identify the optimum band of the EEG μ-rhythm, we estimate the whole range of μ-rhythm by choosing $f_1 = 8$ Hz, $w_1 = 2\pi f_1$ and $f_n = 14$ Hz, $w_n = 2\pi f_n$. The adaptive gain parameter η decides the adaptive rate of the algorithm. The accuracy of estimation also depends on the frequency spacing $\Delta\omega/2\pi$. A small $\Delta\omega$ will increase the number of fundamental frequencies (i.e. weights $\mathbf{w}_k$) and the estimation process will be highly accurate. A very small $\Delta\omega$ also increases the computational complexity. An appropriate value of η should be selected according to (8) for the convergence of the algorithm. The accuracy for various values of $\Delta\omega/2\pi$ and η are analyzed and the findings are presented in Section 3.

2.2. Analysis with BMFLC

In this section, we first present the proposed method for time-frequency decomposition of the rest-EEG and movement-EEG followed by identification of optimal band. The identified optimal band will be later used for better event classification. The block diagram of the procedure is given in Fig. 4. The three steps **A**, **B** and **C** shown in Fig. 4 are organized as three sub-sections for ease of analysis.

2.2.1. Time-frequency decomposition

By construction of BMFLC, the weight vectors $\mathbf{w}_k$ represents the amplitude information of each frequency component at time instant k. This information forms the basis for time-frequency decomposition of the signal. Each amplitude weight represents the magnitude of the corresponding frequency in the signal. The modelled signal with BMFLC at time instant k is given by

$$y_k = \mathbf{w}_k^T \mathbf{x}_k \tag{9}$$

Since the reference vectors $\mathbf{x}_k$ are pre-defined and constant, our analysis will be focused on the weight vector $\mathbf{w}_k$. From (5) and

Please cite this article in press as: Veluvolu KC, et al. Adaptive estimation of EEG-rhythms for optimal band identification in BCI. J Neurosci Methods (2011), doi:10.1016/j.jneumeth.2011.08.035

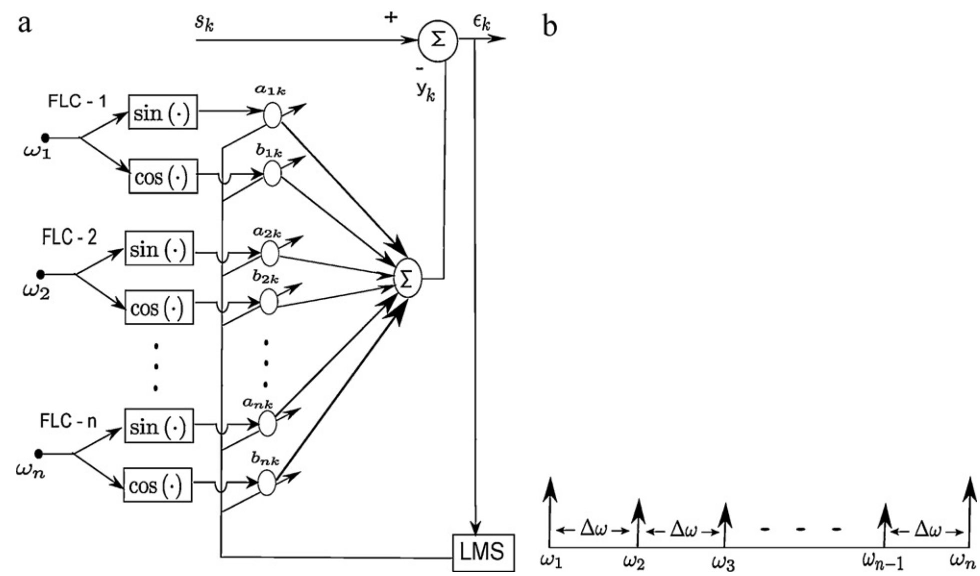

Fig. 3. (a) BMFLC architecture and (b) frequency distribution for multiple FLC's.

architecture in Fig. 3, $\mathbf{w}_k$ contains both the sine and cosine vector terms and so the weight vectors can be re-expressed as

$$\mathbf{w}_k^s = [\,a_{1k} \quad \ldots \quad a_{nk}\,]^T$$
$$\mathbf{w}_k^c = [\,b_{1k} \quad \ldots \quad b_{nk}\,]^T$$

where $\mathbf{w}_k = [\,\mathbf{w}_k^s \quad \mathbf{w}_k^c\,]^T$, $\mathbf{w}_k^s$ and $\mathbf{w}_k^c$ are sine and cosine weights.

In order to evaluate the individual frequency components, we compute the square-root of the sum of squares of the sine and cosine components to obtain

$$\mathbf{w}_k^f = \left[\frac{\sqrt{a_{1k}^2 + b_{1k}^2}}{2} \quad \ldots \quad \frac{\sqrt{a_{nk}^2 + b_{nk}^2}}{2} \right]^T \tag{10}$$

where $\mathbf{w}_k^f$ is the absolute weight vector of the frequency components at instant k. The time-frequency decomposition matrix termed $\mathbf{D}$ can be obtained for the signal with m samples as

$$\mathbf{D} = [\,\mathbf{w}_1^f \quad \ldots \quad \mathbf{w}_k^f \quad \ldots \quad \mathbf{w}_m^f\,] \tag{11}$$

$$= \begin{bmatrix} \frac{\sqrt{a_{11}^2+b_{11}^2}}{2} & \frac{\sqrt{a_{12}^2+b_{12}^2}}{2} & \ldots & \frac{\sqrt{a_{1m}^2+b_{1m}^2}}{2} \\ \frac{\sqrt{a_{21}^2+b_{21}^2}}{2} & \frac{\sqrt{a_{22}^2+b_{22}^2}}{2} & \ldots & \frac{\sqrt{a_{2m}^2+b_{2m}^2}}{2} \\ \vdots & \vdots & \ddots & \vdots \\ \frac{\sqrt{a_{n1}^2+b_{n1}^2}}{2} & \frac{\sqrt{a_{n2}^2+b_{n2}^2}}{2} & \ldots & \frac{\sqrt{a_{nm}^2+b_{nm}^2}}{2} \end{bmatrix} \tag{11}$$

This time-frequency decomposition contains the absolute values of all the frequency components with spacing $\Delta\omega$. These weights are useful to extract the time-frequency characteristics of the EEG signal.

2.2.2. Optimal band selection

The reactive band can be clearly visualized from the time-frequency decomposition of the signal. To quantify the optimal band for the subject, we first analyze spectra power distribution in all the frequency components for rest and each movement class. The square of all the amplitudes of individual frequency components will provide power distribution in each class of a trial and are given by

$$\begin{aligned} \mathbf{P}_{rest} &= \mathbf{D}_{rest} \oplus \mathbf{D}_{rest} \\ \mathbf{P}_{mov} &= \mathbf{D}_{mov} \oplus \mathbf{D}_{mov} \end{aligned} \tag{12}$$

where $\mathbf{P}_{rest}$ and $\mathbf{P}_{mov}$ represent the power distribution matrices for rest and movement. $\mathbf{D}_{mov}$ and $\mathbf{D}_{rest}$ represents the time-frequency decomposition matrix (11) corresponding to rest and movement of the subject. The operator $\oplus$ represents the element by element multiplication of the matrix.

To identify the dominant frequency components, we analyze the average power of all the frequency components. For the above matrices $\mathbf{P}_{rest}$ and $\mathbf{P}_{mov}$, the average power can be obtained by computing the mean of all the rows as each row corresponds to a specific frequency. The difference of the average power distribution between the two matrices will identify the dominant frequency components between two classes (e.g. C3(R) and C3(RH) in a single trial). The difference of the average power can be obtained as

$$\mathbf{P}_{Diff} = avg\{\mathbf{P}_{rest}\} - avg\{\mathbf{P}_{mov}\} \tag{13}$$

where $avg(\cdot)$ is a row operation to compute the mean of every row that corresponds to frequency components ω_i. $\mathbf{P}_{Diff}$ will be a vector with elements corresponding to the power difference of all the

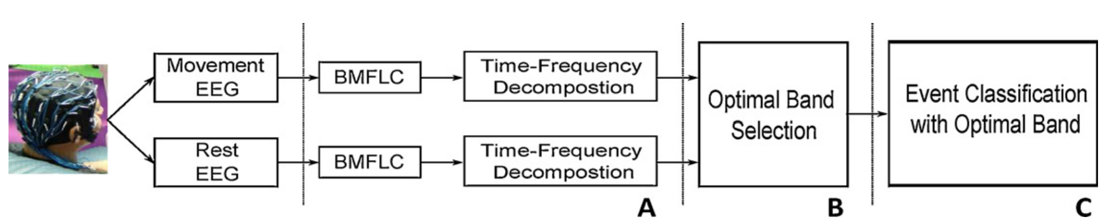

Fig. 4. Flowchart of EEG analysis.

frequency components. This measure will provide power variation in all the frequency components in the μ-band between the two classes under consideration.

The area under the curve $\mathbf{P}_{Diff}$ will provide information about energy distribution between the two movement classes. The region with the maximum energy distribution can be identified for all the movement classes and trials separately and an optimal band can be selected for the subject. The measure to identify the optimal band will be discussed together with the analysis of 30 subjects in Section 3 later.

2.3. Normalized power between events

The classification accuracy depends on the accurate reactive band selection. By considering the most reactive frequency components for each subject the classification accuracy can be improved. In Neuper et al. (2000), it was shown that selection of optimum frequency bands for subjects when compared with standard frequency bands has higher success rate. In this section, we employ the optimum band identified in the previous section for calculation of normalized power.

We first calculate the normalized power (μV^2/Hz) or power spectral density (PSD) with respect to time for the signal in the complete μ-band (8–14 Hz) during rest and movement as follows:

$$\mathbf{C}_{rest} = \frac{sum(\mathbf{P}_{rest})}{BW}, \qquad \mathbf{C}_{mov} = \frac{sum(\mathbf{P}_{mov})}{BW} \tag{14}$$

where the bandwidth $BW = 14 - 8 = 6$ Hz and $sum(\cdot)$ represents the column operation to compute the sum of all components power at instant k.

Similarly, for the EEG signal in the optimum band, the normalized power can be obtained as

$$\mathbf{C}^{+}_{rest} = \frac{sum(\mathbf{P}^{+}_{rest})}{BW^{+}}, \qquad \mathbf{C}^{+}_{mov} = \frac{sum(\mathbf{P}^{+}_{mov})}{BW^{+}} \tag{15}$$

where $\mathbf{P}^{+}_{rest}$ only contains the rows of $\mathbf{P}_{rest}$ that corresponds to the identified optimum band of the subject and BW^{+} represents the identified optimum bandwidth.

To quantify the effect of optimal band selection for all subjects, we analyze the relative power-spectral density. This is necessary as some subjects may have large power (large EEG amplitude) and may lead to bias in the analysis. To accurately quantify the effect of optimal band on the normalized power (PSD) between two events (e.g. C4(LH) and C4(R)), we divide the normalized power (μV^2)/Hz with the average power of the two events (e.g. C4(LH) and C4(R)) to form relative power spectral density (rP/Hz).

3. Results

In this section, we first analyze the accuracy of BMFLC for EEG Estimation. In order to estimate the μ-rhythm, all the data was bandpass filtered in the band of 8–14 Hz. To evaluate the performance of EEG estimation with BMFLC, we employ the root mean square (RMS) defined as $\mathrm{RMS}(s) = \sqrt{(\sum_{k=1}^{m}(s_k)^2)/m}$ where m is the number of samples, s the input signal and s_k input signal at instant k. Percentage accuracy of the performance is quantified as

$$\%\,\mathrm{Accuracy} = \frac{\mathrm{RMS}(s) - \mathrm{RMS}(\epsilon)}{\mathrm{RMS}(s)} \times 100 \tag{16}$$

where ϵ is the error signal. For demonstration, the bandpass filtered EEG μ rhythm in the band of 8–14 Hz when subject #1 is performing movement C4(LH) for a single trial is shown in Fig. 5. In the band of 8–14 Hz, the estimated μ rhythm with $\Delta\omega/2\pi = 0.5$ Hz, $\eta = 0.035$ using BMFLC is also shown in the same figure together with the estimation error. The optimal value of $\eta = 0.035$ ($\eta < 1/n = 1/n = 0.769$) according to condition (8) is chosen for good estimation accuracy. For clarity, a small portion of the signal is presented in Fig. 5. To study the robustness of the algorithm, % accuracy of each trial with all the five classes (see Fig. 1) is computed individually for 30 subjects for different values of $\Delta\omega$ and η. As $\Delta\omega$ decreases, the number of frequency components n increases and the gain parameter η decreases. The mean and standard deviation (±STD) of % accuracy for 30 subjects over 4 trials are tabulated in Table 1. For different values $\Delta\omega$, the optimal values of η are selected. The % accuracy remained constant and it shows the robustness of the algorithm. A value of 0.1–0.5 for $\Delta\omega/2\pi$ is optimum for estimation of μ-rhythm to obtain an accuracy of 96–98%. Also, the mean squared error for all trials and subjects over the signal duration is shown in Fig. 6. For subject # 1, the single trial data in the segment C4(R) (see Fig. 1) is considered for the rest and the data in the segment C4(LH) for the left hand movement. The proposed algorithm is applied separately for both the data with frequency spacing $\Delta\omega/2\pi = 0.5$ Hz and $\eta = 0.035$. The weight vectors of individual frequency components of the EEG rhythm when subject is at rest are shown in Fig. 7(b). The frequency components for the left hand movement C4(LH) are shown in Fig. 7(a). BMFLC inherently divides the time domain signal

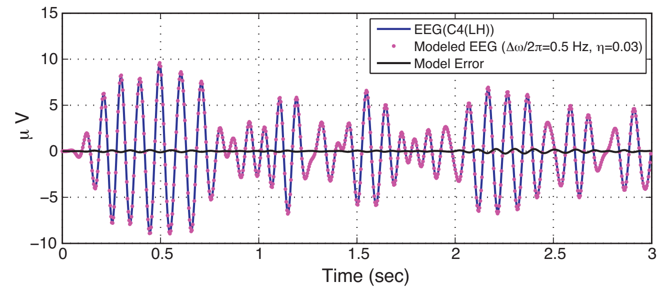

Fig. 5. Subject #1, actual and modeled EEG μ rhythm.

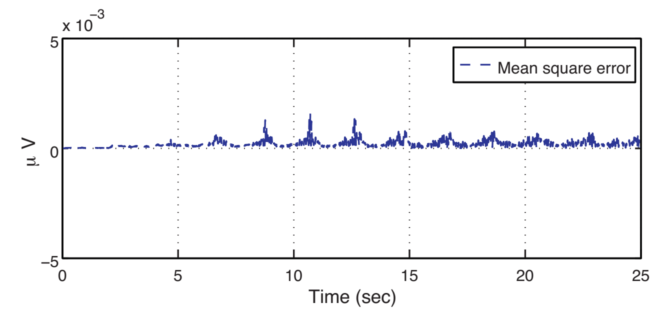

Fig. 6. Mean-squared error over signal duration for all trials/subjects.

Table 1
Accuracy with BMFLC.

30 Subjects × 4 trials (% Accuracy)	$\Delta\omega/2\pi = 0.1$ Hz, $\eta = 0.007$	$\Delta\omega/2\pi = 0.2$ Hz, $\eta = 0.015$	$\Delta\omega/2\pi = 0.4$ Hz, $\eta = 0.03$	$\Delta\omega/2\pi = 0.5$ Hz, $\eta = 0.035$
Average (±STD)	98.85 (±0.03)	98.62 (±0.04)	98.47 (±0.06)	98.34 (±0.05)

Please cite this article in press as: Veluvolu KC, et al. Adaptive estimation of EEG-rhythms for optimal band identification in BCI. J Neurosci Methods (2011), doi:10.1016/j.jneumeth.2011.08.035

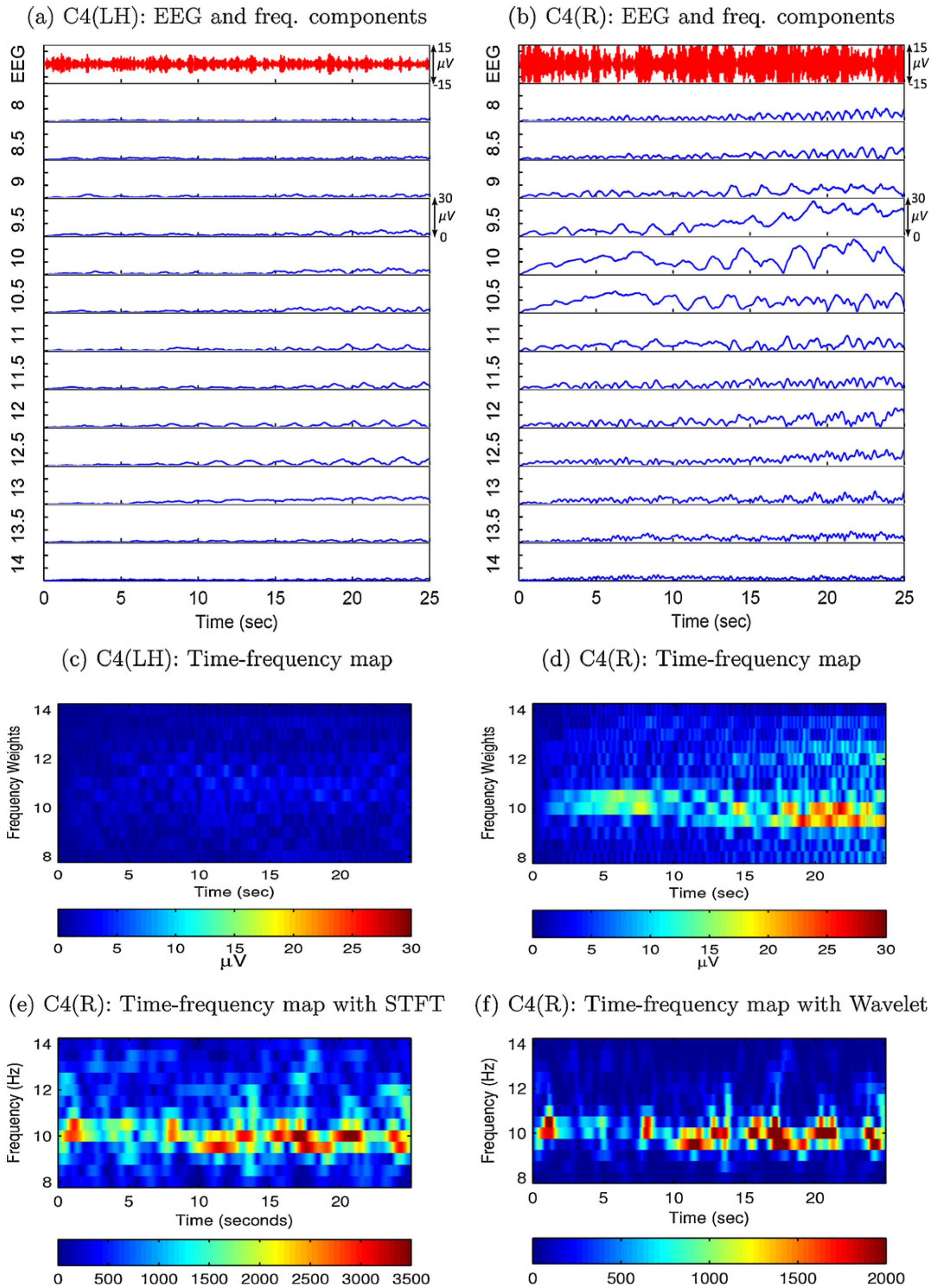

Fig. 7. Subject #1, time-frequency decomposition with BMFLC weights (parameters for the proposed method $\Delta\omega/2\pi = 0.5$ Hz, $\eta = 0.035$).

into individual frequency components. The amplitude of each frequency component gives the strength of the particular frequency in the rhythm and these components corresponds to time-frequency matrix $\mathbf{w}_k^f$. When subject is performing movement, the individual components decrease in the μ-band as shown in Fig. 7(a). The time-frequency decomposition map for the movement C4(LH) and rest C4(R) are shown in Fig. 7(c) and (d) respectively. From the time-frequency decomposition, it can be clearly visualized that the activity is mainly limited to the band 9–11 Hz. Time-frequency decomposition for subject #1, C4(R) using short-time Fourier transform (STFT) and wavelet decomposition are shown in Fig. 7(e) and (f) respectively. For sake of ideal comparison, similar frequency gap is employed with STFT and wavelet transform. Similar reactive band can be identified with all the three methods. Without the need of high computation, BMFLC provides optimal temporal resolution and user-defined frequency resolution $\Delta\omega/2\pi$. Similar analysis is conducted for all events in all the trials for 30 subjects. The analysis revealed similar reactive band characteristics when events C4(RH), C4(RL), C3(LH) and C3(LL) are compared with C4(R) or C3(R). Most of the energy of the signal in the event is confined to a specific reactive band. For illustration, time-frequency maps for subjects #10, #13, #20 with distinct reactive bands are shown

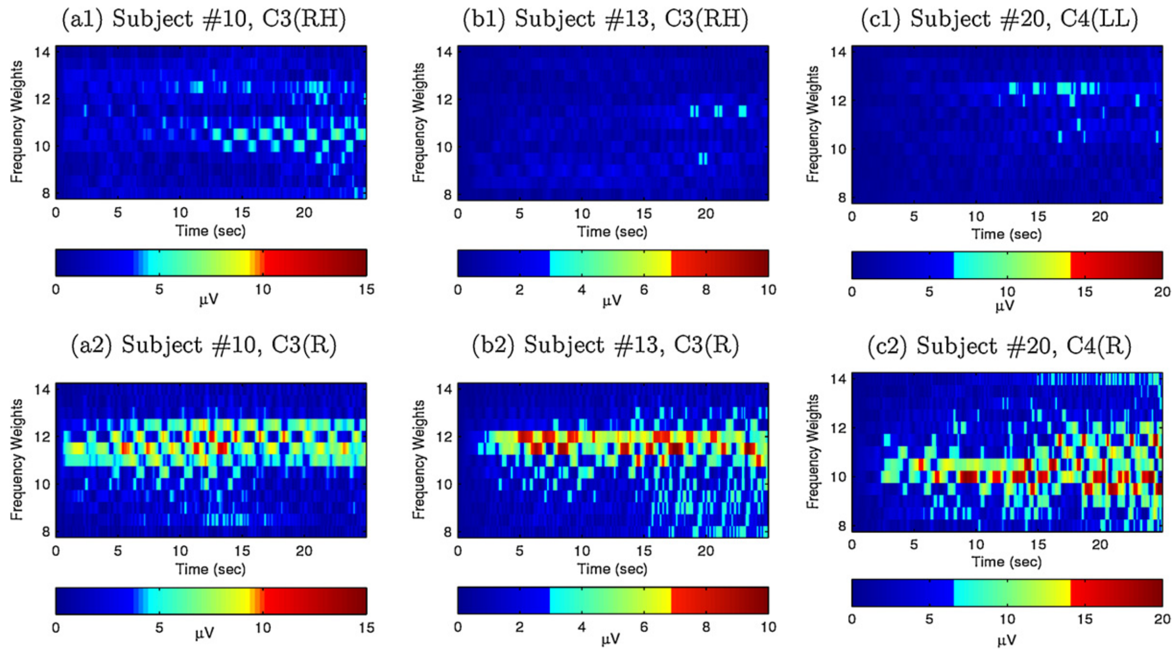

Fig. 8. Time-frequency decomposition for movement and rest.

in Fig. 8 for rest and movement. To identify the optimal band for the subject, $\mathbf{P}_{Diff}$ for all the four movement classes with respect to rest are evaluated for all four trials as discussed in Section 2.2.2. For illustration, the plot of the $\mathbf{P}_{Diff}$ for subject # 1 with all four movement classes with respect to the frequency for a single trial data is shown in Fig. 9(a). From the plot, it is clear that the 9–11 Hz band is reactive for the subject # 1 for all the four movement classes. Plots of $\mathbf{P}_{Diff}$ for 16 subjects for all four movement classes for single trial data are shown in Fig. 9. Most subjects exhibited a distinctive reactive band. To quantify the band and bandwidth for the subject, we first evaluate the distribution (area under the $\mathbf{P}_{Diff}$ curve) for the μ-band and the reactive band. The power ratio % for a movement class in a single trial is defined as

$$P_R = \frac{A_{opt}}{A_\mu} \times 100 \qquad (17)$$

where A_{opt} is the area under the $\mathbf{P}_{Diff}$ curve for the selected reactive band and A_μ is the total positive area under the $\mathbf{P}_{Diff}$ curve for the entire μ-band. Since $\mathbf{P}_{Diff}$ vector represents the average power over a period of time, A_{opt} represents the average power in the optimal band and A_μ represents the average power in the μ-band. P_R also represents % average energy ratio of optimal band to μ-band.

For a selected reactive bandwidth BW^+, the P_R is computed for all the movement classes in all the four trials for the subject. The average P_R resulting from various movement classes and trials for a subject provides the measure of average energy % associated with the selected reactive band and bandwidth. To analyze the effect of bandwidth on P_R, the average P_R for subjects for various bandwidths (2 Hz, 2.5 Hz and 3 Hz) are tabulated in Table 2. The distribution of the subjects in the table reveals that the average P_R of 60–80% exists in most subjects. For only few subjects, an increase in BW^+ increased the energy %. The table shows that most subjects have an average P_R close to 70%. Hence in this study the average P_R = 70% is chosen as the basis to identify the optimal band for the subject. The identified optimal bands for 16 subjects are shown in Fig. 9. The optimal bands shown in Fig. 9 are average of four trials for all movement classes. In Fig. 9, subjects are grouped as good, average, below average and no band subjects. Subjects who displayed a very distinctive common band in all trials are considered as good subjects. In Fig. 9(a)–(e) are marked as good subjects. In Fig. 9(f)–(k) represent the average subjects and all subjects have a common band. However some subjects in one or two trials, a movement class failed to follow the other movement classes (for e.g. Fig. 9(j)–(k)). For some subjects the energy and frequency band depended on the electrode location. For e.g. subject #4 has separate peaks for both electrode locations. However a common band was selected as shown in Fig. 9(h). For some subjects, a large energy difference existed between electrode locations C3 and C4. For e.g. subjects #27 and #7 (see Fig. 9(k)–(m)) show a large difference in power in electrode locations. For subjects #14, #26 a band was not identified in at least 3 trials. Careful observation revealed that the subjects had a power decrease in the μ-band as opposed to power increase as shown in Fig. 9(k)–(m) and are grouped as no band subjects. Few subjects have a reactive bandwidth greater than 2 Hz. For e.g. subject #4 has a reactive band of 9.5–12 Hz.

For some subjects, there was a slight mismatch in the band between two electrode locations C3 and C4. Most subjects displayed a common band for both the C3 and C4 locations. For a given subject, as the reactive band is mainly dependent on the rest C3(R) or C4(R), the band remained constant during all the trials. The reactive band varied from subject to subject, but remained fixed irrespective of the event performed as shown in Fig. 9.

The distribution of optimal band for 30 subjects is shown in Fig. 10(a). Over 93% of the subjects has a distinct reactive band with bandwidth 2 Hz. The study also shows that 40% of the subjects has a reactive band in the range of 9–11 Hz whereas only 8% of the subjects has the reactive band in the range of 12–14 Hz. In Fig. 10(b), the distribution of subjects with different bandwidths is shown. 70% of subjects have a bandwidth of 2 Hz, where as 10% subjects have 2.5 Hz bandwidth. One has to note that the distribution is likely to change with the change of basis measure 70%.

Table 2
Subjects with the optimal band % energy.

Band width	No. of subjects with P_R			
	50–60%	60–70%	70–80%	80–85%
BW^+ = 2 Hz	3	16	8	1
BW^+ = 2.5 Hz	2	13	11	2
BW^+ = 3 Hz	2	12	10	4

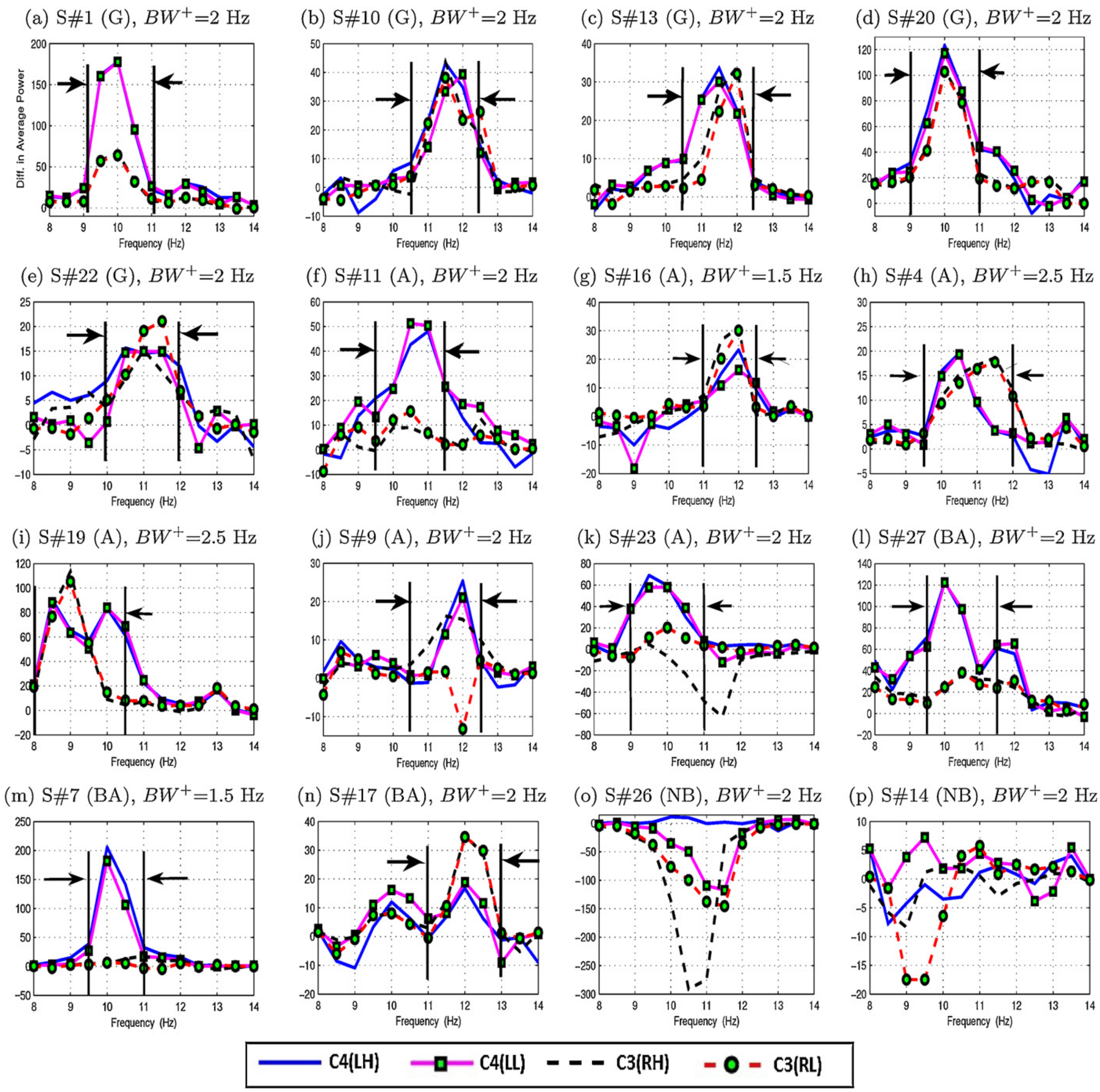

Fig. 9. Plots of $\mathbf{P}_{Diff}$ and optimal band selection in 16 subjects. G, good subjects; A, average subjects; BA, below average subjects; NB, no band subjects.

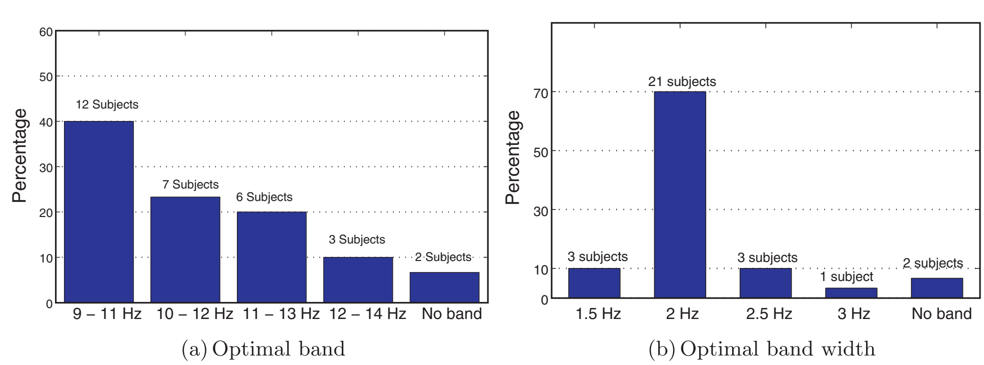

Fig. 10. Optimal band distribution in 30 subjects.

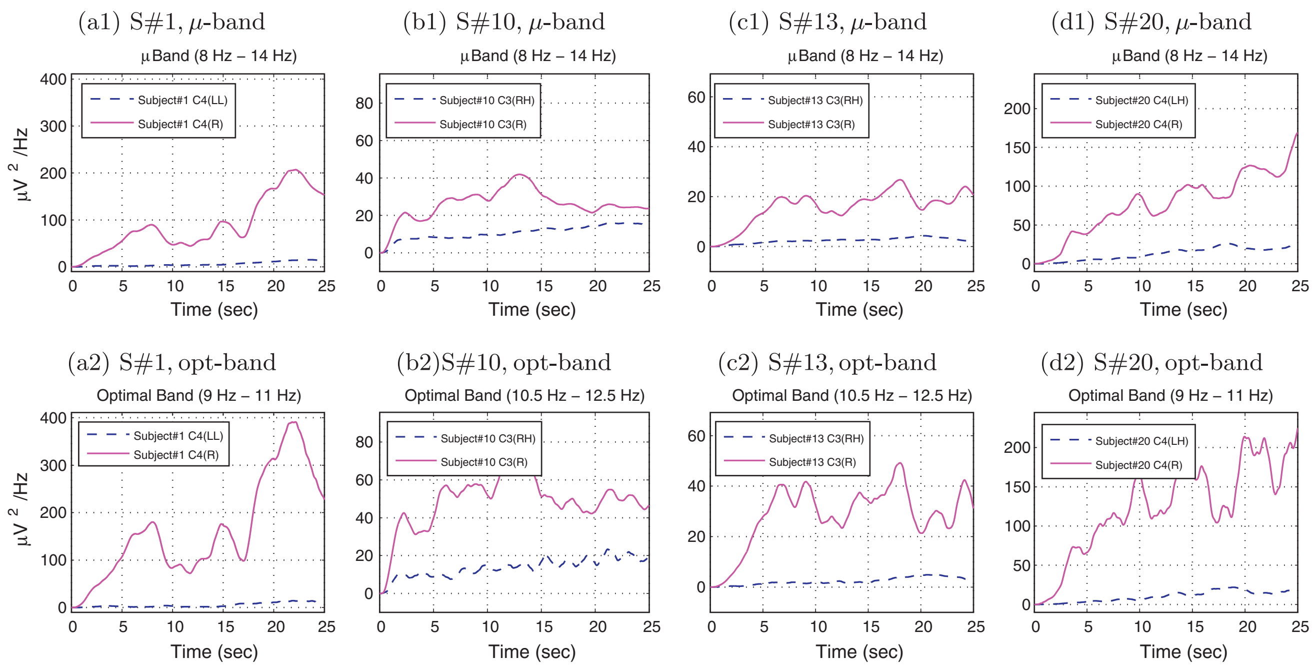

Fig. 11. Normalized power for the μ-band vs. optimal band for single trial data.

Table 3
Comparison of r-power spectral density (rP/Hz) in μ-band and optimal band.

30 subjects× 4 trials	Average of r-power spectral density (rP/Hz)						
	μ-Band (8–14 Hz)			Optimal band			% Increase with optimal band
Event	Rest	Movement	Diff.	Rest	Movement	Diff.	
LH (C4)	11.78 ± 2.1	4.71 ± 2.12	7.06 ± 4.21	31.57 ± 5.61	8.37 ± 4.02	23.19 ± 8.4	228%
LL (C4)	11.62 ± 1.87	4.8 ± 1.87	6.81 ± 3.74	31.13 ± 4.84	8.78 ± 4.19	22.34 ± 7.4	227%
RH (C3)	11.14 ± 2.54	5.28 ± 2.56	5.85 ± 5.1	30.06 ± 4.6	9.15 ± 4.31	20.91 ± 7.96	257%
RL (C3)	11.5 ± 1.84	4.94 ± 1.78	6.53 ± 3.62	29.12 ± 3.99	9.37 ± 3.94	19.75 ± 7.9	202%

As discussed in Section 2.3, the normalized power or power spectral density (PSD) variations are computed for subject #1 C4(R) and C4(LL) events for a single trial and are shown in Fig. 11(a1). The distinction between the rest and left hand motion can be seen in the μ band. With the identified optimal band (9–11 Hz), the difference in normalized power increased as shown in Fig. 11(a2). The difference in normalized power increases by 200% across time with the selection of optimal band. The normalized power variations with optimal bands for subjects #10, #13 and #20 are presented in Fig. 11. The distinction between rest and activity are not very distinct as the characteristics vary from subject to subject. Subject #10 does not have a very clear distinction between C3(RH) and C3(R) in the μ-band as shown in Fig. 11(b1). Selection of the optimal band (10.5–12.5 Hz) increases the power difference by 200% as shown in Fig. 11(b2). To further quantify the effect of optimal band on the normalized power (PSD) we analyze the relative power spectral density (rP/Hz) for all the subjects. The analysis conducted for 30 subjects for four events (LH, LL, RH and RL) in all trials and mean ± standard deviation is tabulated in Table 3. It reveals that the optimum band improves the difference in the relative power spectral density by a minimum 200% with respect to normalized power on an average across the time.

4. Discussion

For many subjects, a significant change in μ-rhythm does exist over the entire band 8–14 Hz. However, closer examination of specific narrower frequency bands for a subject may provide good difference in the activity with the dominant frequency components. Time-frequency decomposition provides more insight about the characteristics of the EEG and dominant frequency components, their time-domain characteristics. The amplitude weights of individual frequency components provide extra information about the subject when compared to conventional methods of calculating the band power using FFT or STFT. The frequency gap $\Delta\omega/2\pi$ in the proposed method can be varied according to the requirement. A small $\Delta\omega/2\pi$ can be selected for high time-frequency resolution. Based on the amplitudes of individual frequency components, the most reactive frequencies for a subject can be identified to improve the threshold level for event classification. This method also provides optimal temporal and user-defined frequency resolution and can be employed for feature extraction in BCI.

Earlier methods for identifying the subject specific reactive bands relied on heuristic based methods and require large number of trials to train the subjects. The proposed method can clearly identify the subjects optimal band for an electrode location with fewer number of trials. A period of 25 s for identification of the band for a movement class was considered to analyze the time-domain characteristics of the reactive band. It was evident from the time-frequency maps that the reactive band indeed remained constant through out the entire time-period.

For most subjects a common optimal band existed for all movement classes. Fig. 9 shows that all the four movement classes have a common band. In most of the earlier studies, bandwidth of 3 Hz was employed to customize the reactive band based on heuristic methods. The selection of proper optimal band depends on the subject's energy distribution and an exact band cannot be quantified directly. In this paper, a basis measure of 70% is employed to identify the subject-specific optimal band. A larger band can be employed for all subjects, but it will eventually decrease the power spectral density. Although the analysis in the paper is limited to actual movement-related data, the proposed method will be useful for identifying the optimal band related to movement-imagery for BCI applications. Similar results may not be obtained with imagined movement, however a good difference in power spectral density can be obtained with a proper selection of optimal band with the proposed method.

The proposed method of optimal band identification can be employed for identifying users with a narrow reactive band. The users with a narrow frequency band will operate BCI with higher accuracy compared to subjects without a band. The proposed method in combination with spatial filtering will provide optimal temporal, spatial and time-resolution for real-time feature extraction in BCI's. Identifying the optimal bands in μ and β-bands separately for each electrode location will improve the performance of classifiers. Although the analysis has been limited to μ-band in this paper, the same approach can be extended to β-band to identify the optimal band in β-band for electrode locations. Similar optimal bands for subjects can also be identified with traditional methods like STFT and Wavelet transform.

Results are illustrated for 16 subjects for optimal band identification. Our study reveals that optimal band exists in most subjects and it improves the spectral power density difference between rest and movement. The study clearly identified the optimal band for the subjects and the optimal band can be selected for better event classification. An average of 200% improvement in power spectral density with respect to normalized power can be obtained with the proposed method.

Acknowledgements

Authors would like to thank anonymous reviewers for their valuable suggestions/comments that largely improved the quality of the paper.

References

Akim M, Kiymik M. Application of periodogram and ar spectral analysis to eeg signals. J Med Syst 2000;24(4):247–56.

Allen DP, MacKinnon CD. Time-frequency analysis of movement-related spectral power in eeg during repetitive movements: a comparison of methods. J Neurosci Meth 2010;186:107–15.

Bashashati A, Fatourechi M, Ward RK. A survey of signal processing algorithms in brain–computer interfaces based on electrical signals. J Neural Eng 2007;4: R03.

Birbaumer N, Ghanayim N, Hinterberger T, Iversen I, Kotchoubey B, Kübler A, et al. Guest editorial brain–computer interface technology: a review of the second international meeting. Nature 1999;398(6725):297–8.

Blankertz B, Tomioka R, Lemma S, Kawanabe M, Muller KR. Optimizing spatial filters for robust eeg single-trial analysis. IEEE Signal Proc Mag 2008;25(1): 41–56.

Brunner C, Allison BZ, Krusienski DJ, Vera Kaiser, Mller-Putz GR, Pfurtscheller G, et al. Improved signal processing approaches in an offline simulation of a hybrid brain–computer interface. J Neurosci Meth 2010;188(1):165–73.

Editorial comment. Is this the bionic man? Nature 2006;442(7099):109.

Curran EA, Strokes MJ. Learning to control brain activity: a review of the production and control of eeg components for driving brain–computer interface (bci) systems. Brain Cogn 2003;51:326–36.

Graimann B, Allison B, Pfurscheller G. Brain–computer interfaces. London, UK: Springer; 2010.

Guger C, Edlinger G, Harkam W, Niedermayer I, Pfurtscheller G. How many people are able to operate an eeg-based brain–computer interface (bci)? IEEE Trans Neural Syst Rehabil Eng 2003;11(2):99–110.

Jasper HH. The ten–twenty electrode system of the international federation. Electroen Clin Neuro 1958;10:371–5.

Krusienski DJ, Schalk G, McFarland DJ, Wolpaw JR. A mu-rhythm matched filter for continuous control of a brain–computer interface. IEEE Trans Biomed Eng 2007;54(2):273–80.

Lotte F, Congedo M, Lecuyer A, Lamarche F, Arnaldil B. A review of classification algorithms for EEG-based brain–computer interfaces. J Neural Eng 2007;4:R1–13.

McFarland DJ, Lefkowicz AT, Wolpaw JR. Design and operation of an eeg-based brain–computer interface (bci) with digital signal processing technology. Behav Res Meth Instrum Comput 1997;29:337–45.

McFarland DJ, Wolpaw JR. Sensorimotor rhythm-based brain–computer interface (bci): model order selection for autoregressive spectral analysis. J Neural Eng 2008;5:6.

McFarland DJ, Anderson CW, Muller KR, Schlogl A, Krusienski DJ. Bci meeting 2005 – workshop on bci signal processing: feature extraction and translation. IEEE Trans Neural Syst Rehabil Eng 2008;14(2):135–8.

McFarland DJ, Sarnacki WA, Wolpaw JR. Electroencephalographic (eeg) control of three-dimensional movement. J Neural Eng 2010;7:36007.

Mueller-Putz GR, Scherer R, Pfurtscheller G, Rupp R. Eeg-based neuroprosthesis control: a step towards clinical practice. Neurosci Lett 2000;382:169–74.

Mueller-Putz GR, Scherer R, Pfurtscheller G, Rupp R. Brain–computer interfaces for control of neuroprosthesis: from sysnchronous to asynchronous mode of operation. Biomed Eng 2006;51(2):57–63.

Neuper C, Mueller-Putz GR, Scherer R, Pfurtscheller G. Motor imagery and eeg-based control of spelling devices and neuroprostheses. Prog Brain Res 2000:159393–409.

Pfurtscheller G, Neuper C. Motor imagery activates primary sensorimotor area in humans. Neurosci Lett 2000;239:65–8.

Pfurtscheller G, Neuper C, Andrew C, Edlinger G. Foot and hand area mu rhythms. Int J Psychophysiol 2000;26(1–3):121–35.

Pineda AJ, Allison BZ, Vankov A. The effects of self-movement, observation and imagination on μ rhythms and readiness potentials (rp's): toward a brain–computer interface (bci). IEEE Trans Rehabil Eng 2000;8(2):219–22.

Royer SA, Doud AJ, Rose ML, Bin He. Eeg control of a virtual helicopter in 3-dimensional space using intelligent control strategies. IEEE Trans Neural Syst Rehabil Eng 2000;18(6):581–9.

Schalk G, Mellinger J. A practical guide to brain–computer intefacing with BCI2000. London, UK: Springer; 2010.

Sun S, Zhang C, Lu Y. The random electrode selection ensemble for eeg signal classification. Pattern Rcogn 2000;41:1663–75.

Vaughan TM. Guest editorial brain–computer interface technology: a review of the second international meeting. IEEE Trans Neural Syst Rehabil Eng 2000;11(2):94–109.

Vaz C, Thakor N. Adaptive fourier estimation of time-varying evoked potentials. IEEE Trans Biomed Eng 2000;36(4):448–55.

Vaz C, Kong X, Thakor N. An adaptive estimation of periodic signals using a fourier linear combiner. IEEE Trans Signal Process 2000;42(1):1–10.

Veluvolu KC, Ang WT. Estimation and filtering of physiological tremor for surgical robotics applications. Int J Med Robot Comput Assist Surg 2000;6(3):334–42.

Widrow B, Stearns SD. Adaptive signal processing. Englewood Cliffs, NJ: Prentice-Hall; 1985.

Wolpaw JR, McFarland DJ, Vaughan TM. Brain–computer interface research at the wadsworth center. IEEE Trans Rehabil Eng 2000;8(2):222–6.

Wolpaw JR, Birbaumer N, McFarland DJ, Pfurtscheller G, Vaughan TM. Brain–computer interfaces for communication and control. Clin Neurophysiol 2000;113:767–91.

Please cite this article in press as: Veluvolu KC, et al. Adaptive estimation of EEG-rhythms for optimal band identification in BCI. J Neurosci Methods (2011), doi:10.1016/j.jneumeth.2011.08.035